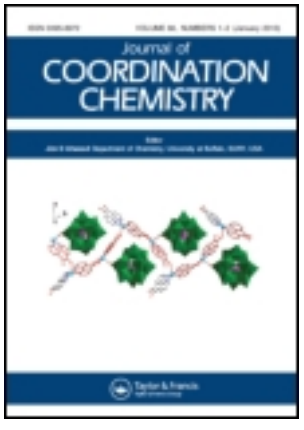

Journal of Coordination Chemistry
Publication details, including instructions for authors and subscription information:
http://www.tandfonline.com/loi/gcoo20

Synthesis and characterization of a new tin(IV) complex for fabrication of an organic light-emitting diode (OLED) and photoluminescence properties of the tin oxide core

Ezzatollah Najafi [a], Mostafa M. Amini [a], Leila Masoomi [a], Saied Saeed Hosseiny Davarani [a], Mohammad Janghouri [b], Ezeddine Mohajerani [b] & Seik Weng Ng [c]

[a] Department of Chemistry, Shahid Beheshti University, G.C., Tehran, Iran

[b] Laser Research Institute, Shahid Beheshti University, G.C., Tehran, Iran

[c] Department of Chemistry, University of Malaya, Kuala Lumpur, Malaysia

Accepted author version posted online: 14 Jun 2013.Published online: 16 Jul 2013.

To cite this article: Ezzatollah Najafi, Mostafa M. Amini, Leila Masoomi, Saied Saeed Hosseiny Davarani, Mohammad Janghouri, Ezeddine Mohajerani & Seik Weng Ng (2013) Synthesis and characterization of a new tin(IV) complex for fabrication of an organic light-emitting diode (OLED) and photoluminescence properties of the tin oxide core, Journal of Coordination Chemistry, 66:15, 2712-2725, DOI: 10.1080/00958972.2013.813940

To link to this article: http://dx.doi.org/10.1080/00958972.2013.813940

Journal of Coordination Chemistry, 2013
Vol. 66, No. 15, 2712–2725, http://dx.doi.org/10.1080/00958972.2013.813940

Synthesis and characterization of a new tin(IV) complex for fabrication of an organic light-emitting diode (OLED) and photoluminescence properties of the tin oxide core

EZZATOLLAH NAJAFI†, MOSTAFA M. AMINI*†, LEILA MASOOMI†, SAIED SAEED HOSSEINY DAVARANI†, MOHAMMAD JANGHOURI‡, EZEDDINE MOHAJERANI‡ and SEIK WENG NG§

†Department of Chemistry, Shahid Beheshti University, G.C., Tehran, Iran
‡Laser Research Institute, Shahid Beheshti University, G.C., Tehran, Iran
§Department of Chemistry, University of Malaya, Kuala Lumpur, Malaysia

(*Received 14 December 2012; in final form 23 April 2013*)

A new tin(IV) complex, $(C_{13}H_{10}NO)[SnCl_4(C_9H_6NO)]\cdot 2CH_3OH$, was prepared in a facile process and characterized by ^1H, ^{13}C, and ^{119}Sn NMR, IR, and UV spectroscopy in addition to single-crystal X-ray diffraction analysis. Current–voltage (I–V) characteristics, photoluminescence (PL), and electroluminescence (EL) properties of the complex have been investigated and an application of the prepared complex in fabrication of an organic light-emitting diode has been demonstrated. The EL of the compound exhibits blue–green emission at 494 nm. Tin(IV) oxide core that resulted from direct thermal decomposition of the complex at 450 °C in air was characterized by X-ray powder diffraction and scanning electron microscopy; then, the PL property was investigated and compared with the PL of the complex. The tin(IV) oxide core showed a band gap of ~3.81 eV determined from the UV/visible absorption spectrum. The tin oxide core showed stable PL with one emission peak centered at 581 nm.

Keywords: Tin(IV) complex; Tin oxide; Photoluminescence; Electroluminescence; OLED

1. Introduction

Luminescent metallocomplexes became an active area of research because of their important commercial applications such as organic light-emitting diodes (OLED), lasers, and fluorescent sensors for highly specific probes [1–4]. Generally, several factors are important in the emission properties of metallocomplexes, including electronic properties of the ligand, metal ion, and coordination geometry. These factors affect the energy mixing and splitting of the electronic states involved in the emission [5–10]. Considerable effort has been devoted to the combination of proper ligands and metal ions to prepare electronic materials in the fabrication of convenient and low-cost OLEDs [11–15]. 8-Hydroxyquinoline (HQ) and its

*Corresponding author. Email: m-pouramini@sbu.ac.ir

derivatives are versatile ligands towards a range of metal ions and possess useful photophysical properties with a triplet state located at 17,100 cm^{-1} (585 nm). Metal complexes of 8-hydroxyquinolinates have been considered as a promising material for the design of electroluminescent devices. Many efforts have been devoted to understand the correlation between electronic structure and photonic properties of the 8-HQ derivatives of main and transition metal ions, and a number of complexes with excellent luminescent properties have been prepared [16–20]. However, the photoluminescence (PL) behavior of the 8-HQ derivatives of group IVA in general and tin(IV) in particular have not yet been thoroughly investigated.

Tin has variable valance states (divalent and tetravalent) and coordination structures. Furthermore, tin has a higher work function relative to groups IIB and IIIA [21]; hence, tin complexes have higher ionization potential than other metal complexes. Therefore, synthesis of the 8-HQ complexes of tin for luminescent studies and use in fabrication of OLED devices should be interesting. In continuation of our interest in PL studies of 8-HQ complexes of tin, here we report the synthesis, characterization, and PL studies of a new tin complex of hydroxyquinoline, demonstrate the utilization of it in the fabrication of an electroluminescent device, and study the PL properties of tin oxide core obtained from direct thermal decomposition of the complex at 450 °C.

Semiconductor nanoparticles have attracted attention because of their unique electronic, magnetic, and optical properties [22]. Among various semiconductor materials, tin oxide, a prototypical transparent n-type semiconductor with a wide band gap ($E_{gap} = 3.6$ eV at 300 K), possesses interesting optical, dielectric, and catalytic properties. This has resulted in many industrial applications, such as catalyst support, transparent conducting electrodes, and gas sensor [23, 24]. This material has advantages, including high thermodynamic stability in air (at least up to 500 °C), low cost, and a possibility of introducing catalysts or dopants to enhance the sensitivity or selectivity [25]. Several methods have been employed for the preparation of nanoscale tin oxide particles, including vapor phase growth, vapor–liquid–solid processes, electrodeposition, electron beam evaporation, sputtering of Sn targets, hydrothermal, reaction in liquid ammonia, pulsed laser deposition, mechano chemical, and sol gel precipitation [26–28]. In this paper a tin complex, $(C_{13}H_{10}NO)[SnCl_4(C_9H_6NO)]\cdot 2CH_3OH$, has been prepared and used as a precursor for the preparation of tin oxide nanoparticles. The tin oxide nanoparticles have been obtained easily based on the rapid thermolysis of the tin complex in air. This is the first report on the synthesis of nanosized tin oxide by this type of tin complex, showing that tin compounds can be suitable precursors for the preparation of desired nanoscale tin oxide. The synthetic method is convenient and the product has good monodispersity in comparison with wet chemical routes such as sol–gel, and the present method does not require stabilizers. Relative to the tin oxide prepared by thermal evaporation, this tin oxide has a narrow and uniform shape, and when compared to the sonochemical method, the sizes of the nanoparticles in this study are larger. There is no particle aggregation and the nanoparticles are clearly distinct.

Properties of semiconductor nanoparticles, especially the photoluminescent properties, have been a subject of extensive investigations [29]. Optical measurements such as optical band gap and PL are very important parameters for the determination of the structure, defects, and impurities of nanostructure materials [30]. In this work, the tin oxide nanoparticles prepared from the thermolysis of tin complex were characterized by X-ray powder diffraction (XRD) and scanning electron microscopy, and its PL was compared to the original complex.

2. Experimental

2.1. *Materials and instrumentation*

8-HQ and stannic tetrachloride pentahydrate were purchased from Merck, and 10-hydroxybenzo[h]quinoline (HBQ), poly(3,4-ethylenedi-oxythiophene) (PEDOT), poly(styrenesulfonate) (PSS), (2-(4-biphenyl)-5-(4-t-butyl-phenyl)-1,3,4-oxadiazole) (PBD), and PVK (polyvinyl carbazole) were obtained from Aldrich and used without purification. All solvents were dried and distilled under nitrogen prior to use, according to the standard procedure.

Melting point was obtained with an Electrothermal 9200 melting point apparatus and is not corrected. Infrared spectra from 4000–250 cm^{-1} were recorded on a Shimadzu 470 FT-IR instrument using KBr pellets. ^{1}H, ^{13}C, and ^{119}Sn NMR spectra were recorded at room temperature in DMSO on Bruker AVANCE 300-MHz operating at 300.3, 75.4, and 111.9 MHz, respectively. Elemental analysis was performed with a Thermo Finnigan Flash-1112EA microanalyzer. Electroluminescence (EL) and PL spectra of a fabricated OLED were obtained on HR4000 Oceanoptic and USB2000 spectrometers, respectively. The current–voltage and luminance were checked by Keithley 2400 and Minolta Luminance meter LS110. The thickness of the sample was measured using a DekTak 8000 profilometer. UV–vis spectra were recorded on a HR4000 Oceanoptic spectrometer using a 1.0 cm path length cell at room temperature. X-ray diffraction pattern was obtained on a STOE diffractometer with Cu Kα radiation. The morphology was observed on a VEGA II TESCAN scanning electron microscope with gold coating. Cyclic voltammetry measurements were carried out on a μ-Autolab III electrochemical workstation with CH_2Cl_2 solution containing 0.1 M supporting electrolyte of tetrabutyl ammonium perchlorate in a three-electrode cell, where glassy carbon, Pt wire, and Ag/Ag^{+} were used as the working electrode, counter electrode, and reference electrode, respectively. Ferrocene was added as an internal standard after each set of measurements and all the potentials reported were quoted with reference to the ferrocene–ferrocenium (Fc/Fc^{+}) couple at a scan rate of 100 mV/s.

2.2. *X-ray crystallography*

Single-crystal X-ray diffraction data were collected on a Bruker SMART APEX at 100 K with a graphite monochromated Mo-Kα radiation using APEX2 software [31]. Data were collected to a maximum 2θ value of 27.62°. Cell constants and an orientation matrix for the data collection were obtained by least-squares refinement of diffraction data from 4560 unique reflections. A numerical absorption correction was applied using X-SHAPE software [32]. The structure was solved by direct methods and refined on F^2 using a full-matrix least-squares procedure with anisotropic displacement parameters [33]. All refinements were performed using the SHELXL97 crystallographic software package [34]. Crystal data and refinement details for the complex are listed in table 1.

2.3. *Preparation of 10-hydroxybenzo[h]quinolinium tetrachloro(quinolin-8-olato) stannate(IV) methanol disolvate*

Stannic chloride pentahydrate (0.35 g, 1.0 mM), 10-hydroxybenzo[h]quinoline (0.20 g, 1.0 mM), and 8-HQ (0.15 g, 1.0 mM) were loaded into a tube with a side arm and then

Table 1. Crystal data and refinement details for the complex.

Molecular formula	$C_{24}H_{24}Cl_4N_2O_4Sn$
Formula weight	664.94
Crystal size (mm)	$0.25 \times 0.20 \times 0.15$
Crystal color	Yellow
Wavelength (Å)	0.71073
Crystal system	Triclinic
Space group	$P\bar{1}$
a (Å)	7.5298(4)
b (Å)	9.9059(3)
c (Å)	17.8457(7)
α (°)	98.202(3)
β (°)	98.667(4)
γ (°)	98.417(4)
V (Å^3)	1283.13(9)
Z	2
$F(0\ 0\ 0)$	664
Limiting indices	$-9 \leqslant h \leqslant 9$ $-12 \leqslant k \leqslant 12$ $-23 \leqslant l \leqslant 23$
Calculated density (mg/m^3)	1.721
Absorption coefficient (mm^{-1})	1.447
θ range (°)	2.58–27.62
Goodness of fit on F^2	1.071
Data/restraints/parameters	0.985/0/321
Final R indices [$I > 2\sigma(I)$]	$R_1 = 0.0498$, $wR_2 = 0.1164$

filled with dry methanol and sealed. The tube was kept at 60 °C and yellow crystals were collected from the cold side arm tube after two weeks. Yield: 80%. m.p., 245–247 °C). $C_{22}H_{16}Cl_4N_2O_2Sn$ (600.89): Calcd (%) C 43.98, H 2.68, N 4.66; found: C 43.85, H 2.72, N 4.92. M.p. = 245–247 °C. IR (KBr, cm^{-1}): 3547 (ν O–H), 3094 (ν C–H), 1593 (ν C=C), 423 (ν Sn–N), 391 (ν Sn–O). ^{1}H NMR (DMSO): δ 7.18 (H-19), 7.28 (H-7, $^4J^{119}Sn$–$^1H = 32$), 7.37 (H-18), 7.52 (H-2, $^4J^{119}Sn$–$^1H = 23$), 7.42 (H-6), 7.68 (H-5), 7.71 (H-17), 7.74 (H-14), 8 (H-15), 8.18 (H-12), 8.31 (H-3), 8.62 (H-1, $^3J^{119}Sn$–$^1H = 34$), 9.01 (H-12), 9.18 (H-10), 12.05 (NH). ^{13}C NMR (DMSO): δ 111.2 (C-7, $^3J^{119}Sn$–$^{13}C = 46$), 112.8 (C-19), 117.3 (C-5), 121 (C-17), 121.4 (C-22), 122.1 (C-2, $^3J^{119}Sn$–$^{13}C = 42$), 124.2 (C-21), 125.2 (C-11), 126.1 (C-13, C-18), 126.5 (C-14), 126.7 (C-6), 127.6 (C-15), 129.5 (C-4), 134.3 (C-16), 136.0 (C-3), 137.4 (C-9, $^4J^{119}Sn$–$^{13}C = 31$), 144.5 (C-10), 146.7 (C-12), 150.1 (C-1, $^2J^{119}Sn$–$^{13}C = 53$), 152.4 (C-8), 158.2 (C-20). ^{119}Sn NMR (DMSO): δ −545.6.

2.4. *Preparation of tin oxide nanoparticles*

Title compound (0.66 g, 0.5 mM) was placed in an electric furnace and heated to 450 °C for 4 h. After cooling, a white precipitate was obtained. The IR spectrum and XRD pattern showed that calcination was complete and the organic moiety was decomposed. The solid was then washed with ethanol and dried under nitrogen.

2.5. *Fabrication of OLED by utilization of prepared complex*

For fabricating an OLED from the complex, initially the ITO coated glass substrate was washed thoroughly in an ultrasonic bath by mild soap, distilled water, acetone,

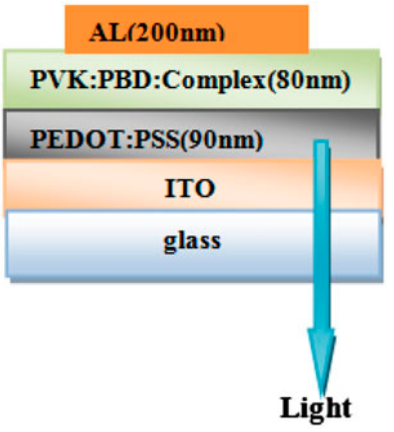

Figure 1. Schematic structure of the OLEDs.

dichloromethane, dichloroethane and methanol. PEDOT : PSS (poly(3,4-ethylenedi-oxythiophene) : poly(styrene- sulfonate)) as a hole-injecting layer was then spin coated on the clean substrate. The required thickness of the layer was 90 nm. The coated layer was then cured at 120 °C to reduce the surface roughness. The emitting layer was then spin coated from a solution of PVK (polyvinyl-carbazole) : PBD (2-(4-biphenyl)-5-(4-t-butyl-phenyl)-1,3,4-oxadiazole):complex at 100 : 40 : 10 weight percent in dichloromethane to make a sample with the following structure: ITO/PEDOT : PSS(90 nm)/PVK : PBD:complex (80 nm)/Al(200 nm). PVK as a hole-transporting material and PBD as an electron-transporting material were doped with the tin compound as an emissive layer. Before thermal vacuum coating of the Al layer, the sample was left in the oven at 120 °C. After coating the Al layer, the sample was left in the vacuum chamber in argon to reduce the risk of oxidation during cooling to room temperature. The active area of the prepared sample was $7 \times 7\,mm^2$. The structure of final sample is shown in figure 1.

3. Results and discussion

3.1. *Synthesis*

Reaction of an appropriate amount of stannic chloride pentahydrate, 10-hydroxybenzo[h] quinoline, and 8-HQ in dry methanol provided the title compound in good yield. This reaction is fast and facile with progress monitored by the appearance of fluorescence color. The compound was characterized by IR, ^{1}H, ^{13}C, and ^{119}Sn NMR spectroscopic analysis in addition to single-crystal X-ray diffraction. The complex readily dissolves in polar solvents such as DMSO and methanol, reflecting its ionic nature.

3.2. *General characterization*

The infrared spectrum of the complex showed stretching vibration of Sn–N at $423\,cm^{-1}$. In the IR spectrum of the complex the presence of Sn–O vibration at $391\,cm^{-1}$ clearly

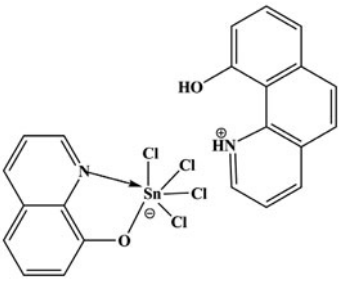

Scheme 1. Line drawing structure of the complex.

indicates deprotonation of the 8-HQ has taken place in coordination to the tin complex. The Sn–Cl symmetric stretching frequency of the complex is at 256 cm^{-1}.

For the determination of structural features of the complex in solution, we obtained ^{1}H, ^{13}C, and ^{119}Sn NMR spectra. The ^{1}H and ^{13}C NMR spectra of the complex (scheme 1) showed the expected aromatic signals with correct integration. The values of $J^{119}Sn–^{1}H$ and $J^{119}Sn–^{13}C$ are obtained according to the literature [35]. The ^{119}Sn NMR spectrum of the complex in DMSO showed only one sharp resonance at −545.6 ppm, within the range of six-coordinate tin [36]. 10-Hydroxybenzo[h]quinoline is more crowded than 8-HQ, the less sterically crowded ligand engages in chelation, and the more crowded ligand is protonated for charge balance; and there is not enough space for the coordination of both ligands simultaneously.

3.3. *Description of crystal structure of 10-hydroxybenzo[h]quinolinium tetrachloro (quinolin-8-olato)stannate(IV)*

The molecular structure and unit cell are shown in figures 2 and 3, respectively, and the selected bond lengths and angles are listed in table 2. The complex is a salt, consisting of four components: a complex anion, $[SnCl_4(C_9H_6NO)]^-$, a cation, (10-hydroxybenzo[h] quinolinium)$^+$, and two lattice methanols which are linked by the electrostatic forces and hydrogen bonds. Although, the quinolin-8-olate anion is involved in a number of complexes with both inorganic tin(IV) and organotin(IV) systems, preparations of mixed chelate complexes are difficult as the compounds disproportionate into symmetrical derivatives. Attempting to prepare a mixed-chelate tin(IV) complex by reacting stannic chloride with 8-HQ and 2-methyl-8-HQ [37] yielded 8-hydroxy-2-methyl quinolinium tetrachloro (quinolin-8-olato)stannate(IV) salt as a methanol solvate. The ligand coordinated is the less sterically crowded one. Similarly, in this study, the reaction of 10-hydroxybenzo[h]quinoline and 8-HQ in methanol yielded the di-solvated salt (scheme 1, figure 2) and, as expected, the less sterically crowded ligand engages in chelation and the more sterically crowded ligand is protonated.

In $[(C_{13}H_{10}NO)][(SnCl_4(C_9H_6NO)]$, the tin(IV) is N,O-chelated by the quinolin-8-olate anion and is further coordinated by four chlorides in a distorted *cis*-$SnNOCl_4$ octahedral coordination. The tin-chloride bonds *trans* to the chelating atoms are significantly shorter than the other tin-chloride bonds. Apparently, the main factor that controls the packing is the presence of weak intra- and inter-molecular interactions. The cations and anions are linked to methanol by O–H···O and N–H···O hydrogen bonds. One molecule functions

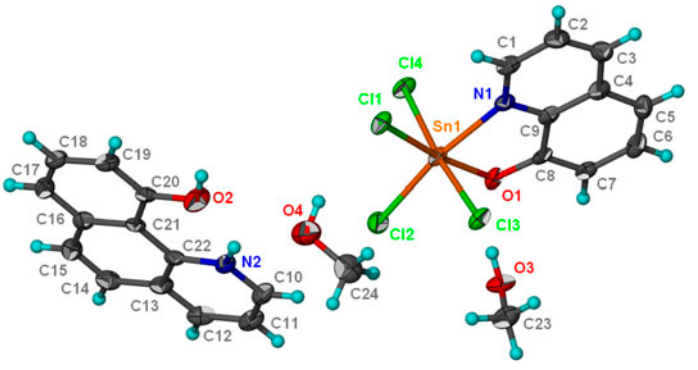

Figure 2. Molecular structure of the complex. Thermal ellipsoids scaled up to 40% probability level.

Table 2. Selected bond distances and angles for the complex.

Bond lengths (Å)		Bond angles (°)	
Sn(1)–O(1)	2.073(3)	O(1)–Sn(1)–Cl(2)	89.57(9)
Sn(1)–N(1)	2.204(4)	O(1)–Sn(1)–N(1)	78.62(13)
Sn(1)–Cl(1)	2.4167(11)	N(1)–Sn(1)–Cl(2)	168.15(10)
Sn(1)–Cl(2)	2.3767(12)	O(1)–Sn(1)–Cl(4)	90.13(9)
Sn(1)–Cl(3)	2.4243(11)	N(1)–Sn(1)–Cl(4)	88.08(9)
Sn(1)–Cl(4)	2.4144(11)	Cl(2)–Sn(1)–Cl(4)	92.99(4)

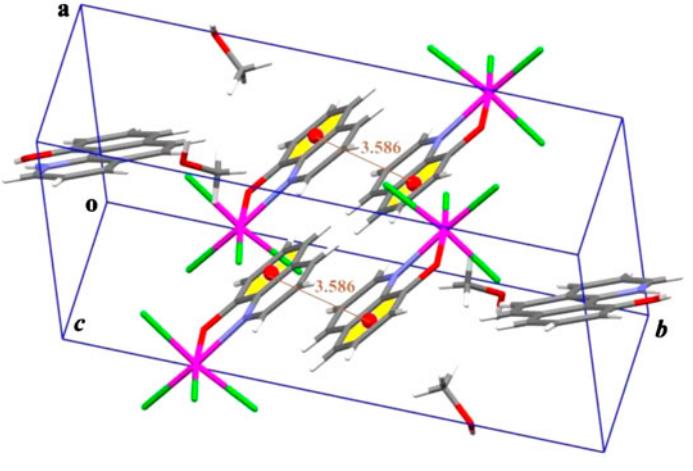

Figure 3. Crystal packing in the complex.

only as an acceptor, whereas the other functions both as a donor and as an acceptor. Hydrogen bonding and face-to-face π–π stacking interactions (figure 3) between phenoxy rings of two adjacent molecules with centroid–centroid distance of 3.58 Å led to a self-templating 2-D supramolecular network.

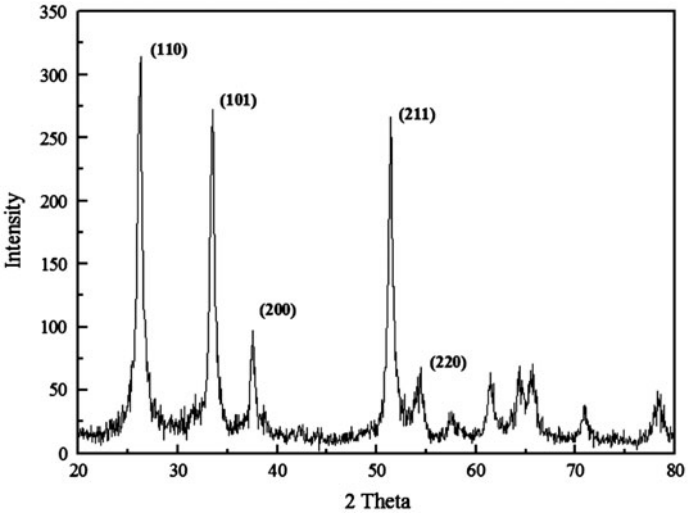

Figure 4. X-ray diffraction pattern of tin oxide prepared by direct calcination of complex.

3.4. *Thermal investigation of prepared complex*

Thermal analysis (TGA–DTA) was employed to study the behavior of the complex during heat treatment (Supplementary material). The complex is stable to ca. 105 °C. The first mass loss between 91 and 117 °C in TGA accompanied with an endothermic peak in the DTA curve is due to the loss of lattice methanol. The second endothermic peak in the DTA curve at 245 °C without the mass loss in TGA curve is associated with complex melting, and the distinct mass loss from 300 to 450 °C with a broad endothermic peak in the DTA curve is attributed to elimination of ligands. Finally, the intense exothermic peak centered at 560 °C in the DTA curve with a slight mass loss above 450 °C is associated with the formation and crystallization of tin oxide. The overall weight loss (75.2%) is in agreement with the calculated value for the formation of tin oxide (74.4%).

3.5. *Preparation of tin(IV) oxide from title compound*

Tin oxide nanoparticles were prepared by direct calcination of the complex at 450 °C in air and have been characterized by XRD. The XRD pattern (figure 4) corresponds to pure tin oxide with a space group of P4/mm and lattice parameters of $a = 4.738$ Å, $c = 3.188$ Å and $Z = 2$ (JCPDS No. 21-1250). No other phase can be detected from the XRD pattern of the sample, which indicates the high purity of tin oxide nanocrystals.

The morphology of tin oxide powder prepared from calcination of complex is shown in Supplementary material. Particle size distribution is broad in the range of about 100–200 nm.

3.6. *Optical properties of prepared complex*

Figure 5 shows the absorption and fluorescence spectra of the prepared complex and bare ligands in methanol. The UV–vis spectra of 8-HQ, 10-hydroxybenzo[h]quinoline, and

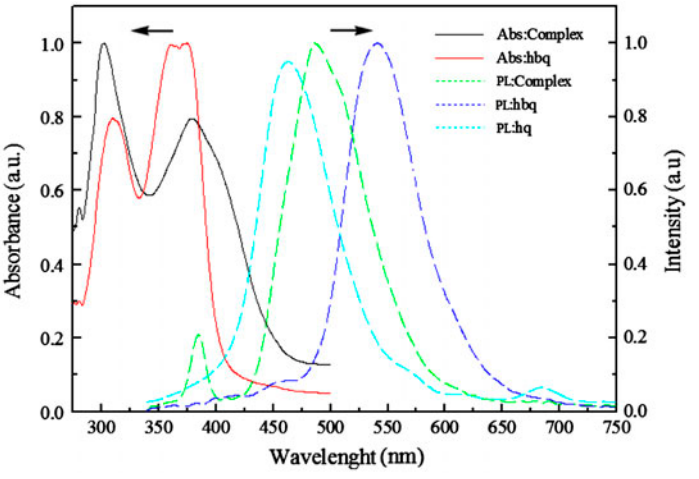

Figure 5. Absorption and fluorescence spectra of the complex in methanol.

complex exhibit bands at 317 nm; 310, 368 nm; and 301, 377 nm, respectively, which can be assigned to $\pi \rightarrow \pi^*$ transitions, and their PL spectra demonstrate broad emissions centered at 463, 540, and 487 nm. There is a 24 nm red-shift and 53 nm blue-shift for the emission spectra of 8-HQ and 10-hydroxybenzo[h]quinoline ligands after coordination. PL emission spectra of ligands and complex have similar shapes. Therefore, one can conclude that the emissions of all compounds originate from $\pi^* \rightarrow \pi$ transitions.

3.7. *Electroluminescence characteristics*

To demonstrate the application of the complex in OLED, this complex was used to fabricate an OLED device and its EL was investigated. To have good energy transfer from host to guest, an overlap between absorption spectrum of the guest and PL spectrum of the host is required. As shown in figure 6, there is a little overlap between the absorption spectrum of the complex as the guest and the PL spectrum of PVK : PBD as the host. Therefore, we expect energy transfer from host to guest to occur to some extent. As shown in figure 7, the EL spectrum of the complex exhibits a blue–green emission around 494 nm with FWHM (full width at half maximum) of 71 nm. This value is close to its PL at 487 nm with about 7 nm red shift in EL spectrum relative to PL spectrum. Similarity of PL and EL supports that blue–green EL originates from the tin complex dopant in the emitting layer of the device, which is formed by the recombination of injected electrons and holes. This can be explained from the energy level diagram of the device (figure 8). The lowest unoccupied molecular orbital (LUMO, electron affinity) and the highest occupied molecular orbital (HOMO, ionization potential) energy levels of the complex were evaluated by cyclic voltammetry on an electrochemical workstation. The oxidation (E_{ox}) and reduction (E_{red}) potentials were used to determine the HOMO and LUMO energy levels using the equations $\mathrm{EHOMO} = -(E_{ox} + 4.8)\,\mathrm{eV}$ and $\mathrm{ELUMO} = -(E_{red} + 4.8)\,\mathrm{eV}$. The E_{ox} and E_{red} potentials were calculated using the internal standard value of ferrocene, -4.8 eV, with respect to vacuum [38]. The results indicate that the ionization potential and the electron affinity of the complex are $\sim$5.8 and $\sim$3.1 eV, respectively. The tin complex has a higher

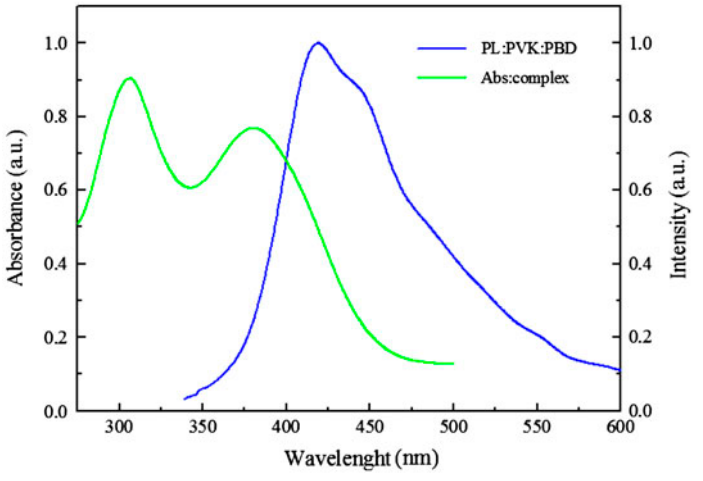

Figure 6. The overlap between absorption spectrum of the complex and PL of PVK : PBD.

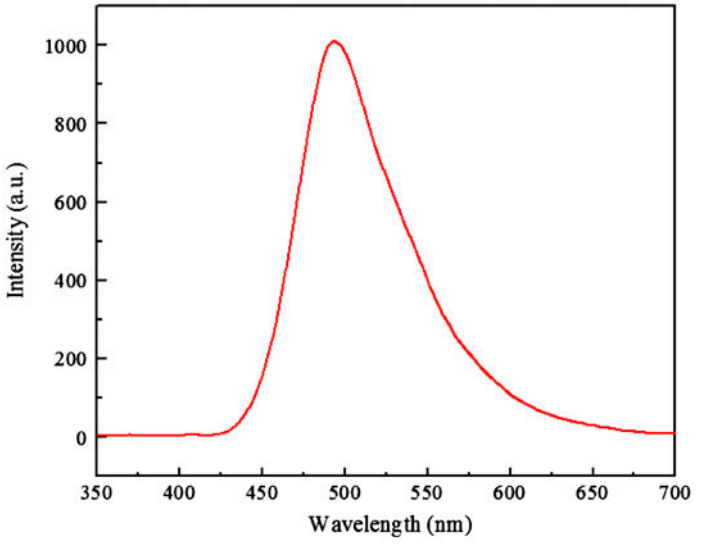

Figure 7. The EL spectrum of the device.

ionization potential than PVK, therefore, it can act as a hole-blocking layer. On the other hand, electrons tunnel into the LUMO energy level of the tin complex and form excitons in the tin complex, then the emissions are realeased. As a result, this tin compound could be used for the fabrication of blue-green OLEDs.

Figure 9 shows the electrical characteristic of OLEDs. The probability of exciton formation in the system has direct relation with the number of holes and electrons in the bulk. Therefore, with reduction in the current density, the probability of exciton formation during operation of the device is reduced. The luminescence–voltage characteristic of the device is shown in figure 10. The maximum brightness of the blue-green emission is at 423 cd/m^2

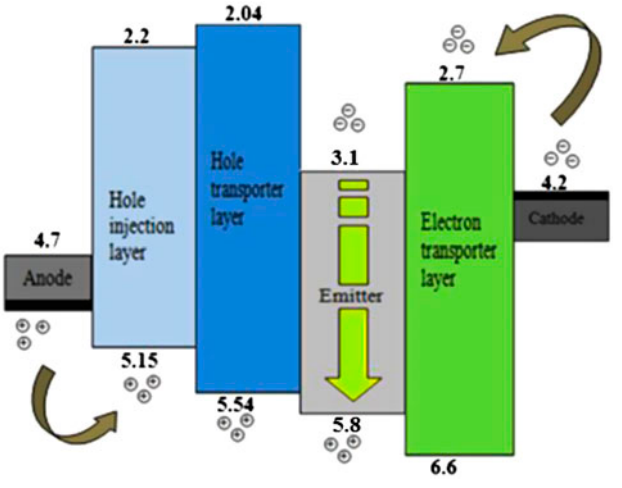

Figure 8. Schematical energy diagram showing the various barriers for charge injection in device. PEDOT : PSS (poly(3,4-ethylenedi-oxythiophene) : poly(styrenesulfonate)) as the hole-injecting layer, PVK (polyvinyl-carbazole) as the hole-transporting layer, and PBD(2-(4-biphenyl)-5-(4-t-butyl-phenyl)-1,3,4-oxadiazole) as the electron-transporting layer.

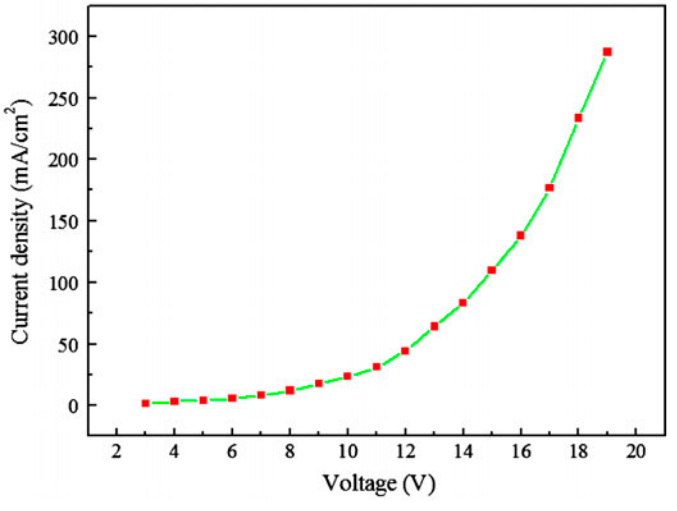

Figure 9. Current–voltage characteristics of the device.

for the device. Finally, the complex showed good thermal stability according to its melting point measurement and TGA-DSC, and is also stable upon exposure to moisture and air. Therefore, a good level of luminance can be sustained with this complex.

3.8. *Optical properties of tin oxide nanoparticles*

Semiconductor nanoparticles with dimensions on the order of bulk exciton will show unique optical properties, which depend strongly on size [39–42]. In semiconductors, band

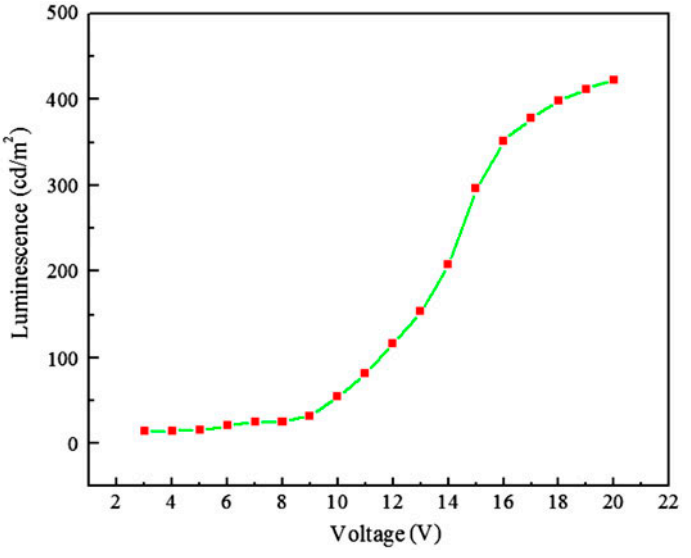

Figure 10. Luminescence–voltage characteristics of the device.

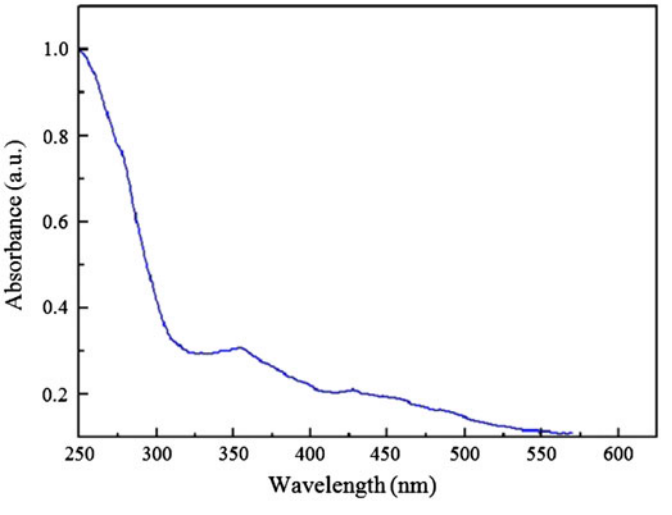

Figure 11. UV/visible absorption spectrum of the tin oxide nanoparticles.

gaps are particle size dependent. Tin oxide is a degenerate semiconductor with band gap energy (Eg) of 3.4–4.6 eV [43]. This scatter in band gap energy of tin oxide may be due to a different extent of non-stoichiometry of the deposited layers. The band gap increases with decreasing particle size and high-energy shift of an absorption edge is generally expected for nanocrystalline materials. The absorption spectrum of the tin oxide nanoparticles calcined at 450 °C is shown in figure 11; the value of the absorption onset of the sample is 325 nm. The absorption onset was blue shifted upon particle growth, indicating that

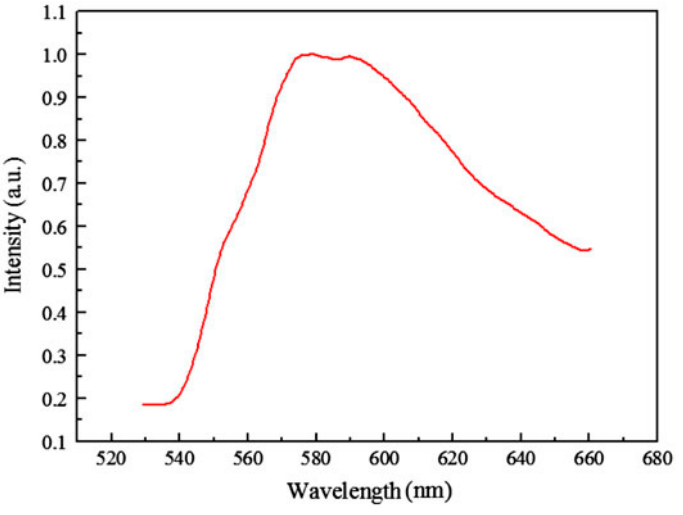

Figure 12. PL spectrum of the tin oxide nanoparticles.

the particles are really in the quantum regime. In this work, the band gap value found for tin oxide nanoparticles (3.81 eV) is larger than that of bulk tin oxide (3.62 eV). Figure 12 shows the PL spectrum of the tin oxide nanoparticles measured at room temperature. The PL spectrum shows an asymmetric, smooth, and broad luminescence band centered at 581 nm.

4. Conclusion

A new tin complex has been synthesized and characterized by spectroscopic techniques and single-crystal structure. The prepared complex showed fluorescence emission at room temperature in solution and has good stability in air and thermally making it suitable for the fabrication of an OLED. EL of the complex showed a yellow emission at 494 nm. Tin oxide nanoparticles were synthesized by the calcination of the tin complex. The room temperature PL spectrum of the tin oxide nanoparticles showed a single emission centered at 581 nm. The band gap of the product is ~(3.81 eV), determined from the UV/visible absorption spectrum. Finally, the results demonstrate that the prepared tin oxide nanoparticles can be used in optoelectronic devices.

Supplementary material

Crystallographic data of $(C_{13}H_{10}NO)[SnCl_4(C_9H_6NO)]\cdot 2CH_3OH$ have been deposited with the Cambridge Crystallographic Data Centre, CCDC No. 895238. These data can be obtained free of charge from the Cambridge Crystallographic Data Centre via www.ccdc.cam.ac.uk/data_request/cif.

Acknowledgment

The authors thank the Vice-President's Office for Research Affairs of Shahid Beheshti University for supporting this work.

References

[1] J.F. Wang, G.E. Jabbour, E.A. Mash, J. Anderson, Y. Zhang, P.A. Lee, N.R. Armstron, N. Peyghambarian, B. Kippelen. *Adv. Mater.*, **11**, 1266 (1999).
[2] R. Pohl, V.A. Montes, J. Shinar, P. Anzenbacher, Jr. *J. Org. Chem.*, **69**, 1723 (2004).
[3] B.W.D. Andrade, J. Brooks, V. Adamovich, M.E. Thompson, S.R. Forrest. *Adv. Mater.*, **14**, 1032 (2002).
[4] J. Slinker, D. Bernards, P.L. Houston, H.D. Abruna, S. Bernhard, G.G. Malliaras. *Chem. Commun.*, **19**, 2392 (2003).
[5] A. Vogler, H. Kunkely. Luminescent Metal Complexes: Diversity of Excited States. In *Topics in Current Chemistry, Vol. 213: Transition Metal and Rare Earth Compounds: Excited States, Transitions and Interactions I*, H. Yersin (Ed.), pp. 143–182, Springer-Verlag, Berlin (2001).
[6] H. Jang, L.M. Do, Y. Kim, J.G. Kim, T. Zyung, Y. Do. *Synth. Met.*, **121**, 1669 (2001).
[7] R. Ballardini, G. Varani, M.T. Indelli, F. Scandola. *Inorg. Chem.*, **25**, 3858 (1986).
[8] J. Yu, Z. Chen, Y. Sakuratani, H. Suzuki, M. Tokita, S. Miyata. *Jpn. J. Appl. Phys.*, **38**, 6762 (1999).
[9] J. Kido, Y. Iizumi. *Chem. Lett.*, **963**, (1997).
[10] Y. Hamada, T. Sano, M. Fujita, T. Fujii, Y. Nishio, K. Shibata. *Jpn. J. Appl. Phys.*, **32**, 514 (1993).
[11] R.H. Holm, M.J. O'Connor. *Prog. Inorg. Chem.*, **14**, 241 (1971).
[12] J. Costamagna, J. Vargas, R. Lattorre, A. Alvarado, G. Mena. *Coord. Chem. Rev.*, **119**, 67 (1992).
[13] A.D. Garnovskii, A.L. Nivorozhkin, V.I. Minkin. *Coord. Chem. Rev.*, **126**, 1 (1993).
[14] P. Guerriero. *Coord. Chem. Rev.*, **139**, 17 (1995).
[15] H. Luo, P.E. Franwick, M.A. Green. *Inorg. Chem.*, **37**, 1127 (1998).
[16] M. Brinkmann, B. Fite, S. Pratontep, C. Chaumont. *Chem. Mater.*, **16**, 4627 (2004).
[17] P.E. Burrows, L.S. Sapochak, D.M. McCarty, S.R. Forrest, M.E. Thompson. *Appl. Phys. Lett.*, **64**, 2718 (1994).
[18] P.E. Burrows, Z. Shen, V. Bulovic, D.M. McCarty, S.R. Forrest, J.A. Cronin, M.E. Thompson. *J. Appl. Phys.*, **79**, 7991 (1996).
[19] L.S. Sapochak, F.E. Benincasa, R.S. Schofield, J.L. Baker, K.K. Riccio, D. Fogarty, H. Kohlmann, K.F. Ferris, P.E. Burrows. *J. Am. Chem. Soc.*, **124**, 6119 (2002).
[20] N.M. Shavaleev, H. Adams, J. Best, R. Edge, S. Navaratnam, J.A. Weinstein. *Inorg. Chem.*, **45**, 9410 (2006).
[21] H.B. Michaelson. *J. Appl. Phys.*, **48**, 4729 (1977).
[22] A.S. Juarez, A. Ortiz. *J. Electrochem. Soc.*, **147**, 3708 (2000).
[23] E.R. Leite, I.T. Weber, E. Longo, J.A. Varela. *Adv. Mater.*, **12**, 966 (2000).
[24] O.K. Varghese, L.K. Malhotra. *Sens. Actuators, B* **19**, 53 (1998).
[25] W. Gopel, K.D. Schierbaum. *Sensors. Actuat. B-Chem.*, **1**, 26 (1995).
[26] Z. Zainal, M.Z. Hussein, A. Kassim, A. Ghazali. *J. Mater. Sci. Lett.*, **16**, 1446 (1997).
[27] G.A. Shaw, I.P. Parkin. *Main Group Met. Chem.*, **19**, 499 (1996).
[28] R. Larciprete, E. Borsella, P. De Padova, P. Perfetti, C. Crotti. *J. Vac. Sci. Technol. A*, **15**, 2492 (1997).
[29] Y. Wang, N. Herron. *J. Phys. Chem.*, **92**, 4988 (1988).
[30] G. Feng, F.W. Shu, K.L. Meng, J.Z. Guang, X. Dong, R.Y. Duo. *J. Phys. Chem. B*, **108**, 8119 (2004).
[31] *X-STEP32, Version1.07b, Stoe & Cie*, Darmstadt, Germany (2000).
[32] G.M. Sheldrick. *SHELX97*, University of Gottingen, Gottingen, Germany (1997).
[33] *X-SHAPE, Version 2.05, Stoe & Cie*, Darmstadt, Germany (2004).
[34] *APEX2 and SAINT*, Bruker AXS, Madison, Wisconsin, USA (2008).
[35] O.G. Tsay, B.K. Kim, T.L. Luu, J. Kwak, D.G. Churchill. *Inorg. Chem.*, **52**, 1991 (2013).
[36] B.D. James, S. Gioskos, S. Chandra, R.J. Magee. *J. Organomet. Chem.*, **436**, 155 (1992).
[37] E. Najafi, M.M. Amini, S.W. Ng. *Acta Cryst. E*, **67**, m241 (2011).
[38] M. Thelakkat, H.W. Schmidt. *Adv. Mater.*, **10**, 219 (1998).
[39] R.S. Ashraf, M. Shahid, E. Klemm, M. Al-Ibrahim, S. Sensfuss. *Macromol. Rapid Commun.*, **27**, 1454 (2006).
[40] F. Kim, S. Connor, H. Song, T. Kuykendall, P.D. Yang. *Angew. Chem. Int. Ed.*, **43**, 3673 (2004).
[41] M.J. Zaworotko, B. Moulton. *Chem. Rev.*, **10**, 2619 (2001).
[42] J.H. He, T.H. Wu, C.L. Hsin, K.M. Li, L.J. Chen, Y.L. Chueh, L.J. Chou, Z.L. Wang. *Small*, **2**, 116 (2006).
[43] P.S. Patil, R.K. Kawar, S.B. Sadale, P.S. Chigare. *Thin Solid Films*, **437**, 34 (2003).